

Further insight into gravitational recoil

Carlos O. Lousto and Yosef Zlochower

*Center for Computational Relativity and Gravitation, School of Mathematical Sciences, Rochester Institute of Technology,
78 Lomb Memorial Drive, Rochester, New York 14623, USA*

(Received 30 August 2007; published 15 February 2008)

We test the accuracy of our recently proposed empirical formula to model the recoil velocity imparted to the merger remnant of spinning, unequal-mass black-hole binaries. We study three families of black-hole binary configurations, all with mass ratio $q = 3/8$ (to nearly maximize the unequal-mass contribution to the kick) and spins aligned (or counter-aligned) with the orbital angular momentum, two with spin configurations chosen to minimize the spin-induced tangential and radial accelerations of the trajectories, respectively, and a third family where the trajectories are significantly altered by spin-orbit coupling. We find good agreement between the measured and predicted recoil velocities for the first two families, and reasonable agreement for the third. We also reexamine our original generic binary configuration that led to the discovery of extremely large spin-driven recoil velocities and inspired our empirical formula, and find rough agreement between the predicted and measured recoil speeds.

DOI: [10.1103/PhysRevD.77.044028](https://doi.org/10.1103/PhysRevD.77.044028)

PACS numbers: 04.25.D-, 04.25.Nx, 04.30.Db, 04.70.Bw

I. INTRODUCTION

Thanks to recent breakthroughs in the full nonlinear numerical evolution of black-hole-binary spacetimes [1–3], it is now possible to accurately simulate the merger process and examine its effects in this highly nonlinear regime [4–18]. Black-hole binaries will radiate between 2% and 8% of their total mass and up to 40% of their angular momenta, depending on the magnitude and direction of the spin components, during the merger [6–8]. In addition, the radiation of net linear momentum by a black-hole binary leads to the recoil of the final remnant hole [19–41], which can have astrophysically important effects [28,40,42–45].

Merging black-hole binaries will radiate net linear momentum if the two black holes are not symmetric. This asymmetry can be due to unequal masses, unequal spins, or a combination of the two. A nonspinning black-hole binary will thus only radiate net linear momentum if the component masses are not equal. However, the maximum recoil in this case (which occurs when the mass ratio is $q \approx 0.36$) is a relatively small $\sim 175 \text{ km s}^{-1}$ [23]. The complementary case, where the black holes have equal masses but unequal spins, was first reported in [27,29]. In the former case the authors calculated the recoil velocity for equal-mass, quasicircular binaries with equal-amplitude, antiparallel spins aligned with the orbital angular momentum direction, while in the latter case the authors used the same general configuration but varied the amplitude of one of the spins. In both the above cases the authors extrapolated a maximum possible recoil (which is tangent to the orbital plane) of $\sim 460 \text{ km s}^{-1}$ when the two holes have maximal spin. At the same time, our group released a paper on the first simulation of generic black-hole binaries with unequal masses and spins, where the spins were not aligned with the orbital angular momentum [28]. That

configuration had a mass ratio of 1:2, with the larger black hole having spin $a/m = 0.885$ pointing 45° below the orbital plane and the smaller hole having negligible spin. The black holes displayed spin precession and spin flips and a measured recoil velocity of 475 km s^{-1} , mostly along the orbital angular momentum direction. It was thus found that the recoil normal to the orbital plane (due to spin components lying in the orbital plane) can be larger than the in-plane recoil originating from either the unequal masses or the spin components normal to the orbital plane. The maximum possible recoil arises from equal-mass, maximally spinning holes with spins in the orbital plane and counter-aligned. This maximum recoil, which will be normal to the orbital plane, is nearly 4000 km s^{-1} .

In [28] we introduced the following heuristic model for the gravitational recoil of a merging binary:

$$\vec{V}_{\text{recoil}}(q, \vec{\alpha}_i) = v_m \hat{e}_1 + v_{\perp} (\cos(\xi) \hat{e}_1 + \sin(\xi) \hat{e}_2) + v_{\parallel} \hat{e}_z, \quad (1)$$

where

$$v_m = A \frac{q^2(1-q)}{(1+q)^5} \left(1 + B \frac{q}{(1+q)^2} \right), \quad (2a)$$

$$v_{\perp} = H \frac{q^2}{(1+q)^5} (\alpha_2^{\parallel} - q \alpha_1^{\parallel}), \quad (2b)$$

$$v_{\parallel} = K \cos(\Theta - \Theta_0) \frac{q^2}{(1+q)^5} |\vec{\alpha}_2^{\perp} - q \vec{\alpha}_1^{\perp}|, \quad (2c)$$

$A = 1.2 \times 10^4 \text{ km s}^{-1}$ [23], $B = -0.93$ [23], here we find $H = (6.9 \pm 0.5) \times 10^3 \text{ km s}^{-1}$, $\vec{\alpha}_i = \vec{S}_i/m_i^2$, \vec{S}_i and m_i are the spin and mass of hole i , $q = m_1/m_2$ is the mass ratio of the smaller to larger mass hole, the index \perp and \parallel refer to perpendicular and parallel to the orbital angular momen-

tum, respectively, at the effective moment of the maximum generation of the recoil (around merger time), \hat{e}_1 , \hat{e}_2 are orthogonal unit vectors in the orbital plane, and ξ measures the angle between the “unequal mass” and “spin” contributions to the recoil velocity in the orbital plane. The angle Θ was defined as the angle between the in-plane component of $\vec{\Delta} \equiv (m_1 + m_2)(\vec{S}_2/m_2 - \vec{S}_1/m_1)$ and the infall direction at merger. The form of Eq. (2a) was proposed in [23,46], while the form of Eqs. (2b) and (2c) was proposed in [28] based on the post-Newtonian expressions in [47]. In Ref. [48] we determined that $K = (6.0 \pm 0.1) \times 10^4 \text{ km s}^{-1}$. Although ξ may in general depend strongly on the configuration, the results of [30] and post-Newtonian calculations show that ξ is 90° for head-on collisions, and the results presented here indicate that $\xi \sim 145^\circ$ for a wide range of quasicircular configurations. A simplified version of Eq. (1) that models the magnitude of V_{recoil} was independently proposed in [32], and a simplified form of Eq. (1) for the equal-mass aligned spin case was proposed in [29].

Our heuristic formula (1) describing the recoil velocity of a black-hole binary remnant as a function of the parameters of the individual holes has been theoretically verified in several ways. In [48] the $\cos\Theta$ dependence was established and was confirmed in [37] for binaries with larger initial separations. In Ref. [36] the decomposition into spin components perpendicular and parallel to the orbital plane was verified, and in [41] it was found that the quadratic-in-spin corrections to the in-plane recoil velocity are less than 20 km s^{-1} .

Consistent and independent recoil velocity calculations have also been obtained for equal-mass binaries with spinning black holes that have spins aligned/counter-aligned with the orbital angular momentum [27,29]. Recoils from the merger of nonprecessing unequal-mass black-hole binaries have been modeled in [32].

The net in-plane remnant recoil velocity arises both from the asymmetry due to unequal masses, which given its $z \rightarrow -z$ symmetric behavior, only contributes to recoil along the orbital plane, and the asymmetry produced by the black-hole spin component perpendicular to the orbital plane. Even if we can parametrize the contribution of each of these two components of the recoil in terms of only one angle, ξ , the modeling of it appears in principle very complicated. ξ may depend on the mass ratio (q) of the holes, as well as their individual spins S_1^z and S_2^z , but also on their orbital parameters such as initial coordinates and momenta, or initial separation and eccentricity. We clearly have to reduce the dimensionality of this parameter space as part of the modeling process. In order to do so, we shall choose a model for ξ that only depends on q and Δ^z for quasicircular orbits. We then perform simulations to determine how accurately this reduced-parameter-space model for ξ reproduces the observed recoil velocities and find that $\xi \approx 145^\circ$, independent of either q or Δ^z .

The paper is organized as follows: in Sec. II we review the numerical techniques used for the evolution of the black-hole binaries and the analysis of the physical quantities extracted at their horizons. In Sec. III we review the post-Newtonian dynamics of binary systems in order to motivate our study of equivalent trajectories for unequal-mass, nonspinning and spinning holes. We focus on four families of such configurations. In Sec. IV we give the initial data parameters for these families. The results of the evolution of those configurations are given in Sec. V, where we also introduce a novel analysis of the trajectories of the punctures and of the waveform phase to model the angle ξ in our heuristic formula Eq. (1). In Sec. VI we analyze new runs of the generic configuration that led us to discover the large recoil velocities produced by the spin projection on the orbital plane of the binary. Here we use more refined tools to analyze the individual hole spins and momenta near merger time, when most of the recoil is generated. We end the paper with a discussion section pointing out the need for further runs with higher accuracy to improve our first results, and an appendix including the post-Newtonian analysis of the maximum recoil configuration.

II. TECHNIQUES

We use the puncture approach [49] along with the `TWOPUNCTURES` [50] thorn to compute initial data. In this approach the 3-metric on the initial slice has the form $\gamma_{ab} = (\psi_{\text{BL}} + u)^4 \delta_{ab}$, where ψ_{BL} is the Brill-Lindquist conformal factor, δ_{ab} is the Euclidean metric, and u is (at least) C^2 on the punctures. The Brill-Lindquist conformal factor is given by $\psi_{\text{BL}} = 1 + \sum_{i=1}^n m_i^p / (2|\vec{r} - \vec{r}_i|)$, where n is the total number of “punctures,” m_i^p is the mass parameter of puncture i (m_i^p is *not* the horizon mass associated with puncture i), and \vec{r}_i is the coordinate location of puncture i . We evolve these black-hole-binary data sets using the `LAZEV` [51] implementation of the moving puncture approach [2]. In our version of the moving puncture approach [2,3] we replace the BSSN [52–54] conformal exponent ϕ , which has logarithmic singularities at the punctures, with the initially C^4 field $\chi = \exp(-4\phi)$. This new variable, along with the other Baumgarte-Shapiro-Shibata-Nakamura (BSSN) variables, will remain finite provided that one uses a suitable choice for the gauge. An alternative approach uses standard finite differencing of ϕ [3].

We use the `Carpet` [55,56] mesh refinement driver to provide a “moving boxes” style mesh refinement. In this approach refined grids of fixed size are arranged about the coordinate centers of both holes. The `Carpet` code then moves these fine grids about the computational domain by following the trajectories of the two black holes.

We obtain accurate, convergent waveforms and horizon parameters by evolving this system in conjunction with a modified $1 + \log$ lapse and a modified Gamma-driver shift condition [2,57], and an initial lapse

$\alpha(t=0) = 2/(1 + \psi_{\text{BL}}^4)$. The lapse and shift are evolved with

$$\partial_t - \beta^i \partial_i \alpha = -2\alpha K, \quad (3a)$$

$$\partial_t \beta^a = B^a, \quad (3b)$$

$$\partial_t B^a = 3/4 \partial_t \tilde{\Gamma}^a - \eta B^a. \quad (3c)$$

These gauge conditions require careful treatment of χ , the inverse of the 3-metric conformal factor, near the puncture in order for the system to remain stable [2,4,12]. In Ref. [58] it was shown that this choice of gauge leads to a strongly hyperbolic evolution system provided that the shift does not become too large.

We use AHFINDERDIRECT [59] to locate apparent horizons. We measure the magnitude of the horizon spin using the isolated horizon algorithm detailed in [60]. This algorithm is based on finding an approximate rotational Killing vector (i.e. an approximate rotational symmetry) on the horizon, and given this approximate Killing vector φ^a , the spin magnitude is

$$S_{[\varphi]} = \frac{1}{8\pi} \oint_{\text{AH}} (\varphi^a R^b K_{ab}) d^2V, \quad (4)$$

where K_{ab} is the extrinsic curvature of the 3D-slice, d^2V is the natural volume element intrinsic to the horizon, and R^a is the outward pointing unit vector normal to the horizon on the 3D-slice. We measure the direction of the spin by finding the coordinate line joining the poles of this Killing vector field using the technique introduced in [8]. Our algorithm for finding the poles of the Killing vector field has an accuracy of $\sim 2^\circ$ (see [8] for details).

We also use an alternative quasilocal measurement of the spin and linear momentum of the individual black holes in the binary that is based on the coordinate rotation and translation vectors [39]. In this approach the spin components of the horizon are given by

$$S_{[i]} = \frac{1}{8\pi} \oint_{\text{AH}} \phi_{[i]}^a R^b K_{ab} d^2V, \quad (5)$$

where $\phi_{[i]}^j = \delta_{\ell j} \delta_{mk} r^m \epsilon^{ijk}$, and $r^m = x^m - x_0^m$ is the coordinate displacement from the centroid of the hole, while the linear momentum is given by

$$P_{[i]} = \frac{1}{8\pi} \oint_{\text{AH}} \xi_{[i]}^a R^b (K_{ab} - K \gamma_{ab}) d^2V, \quad (6)$$

where $\xi_{[i]}^j = \delta_{\ell}^j$.

We measure radiated energy, linear momentum, and angular momentum, in terms of ψ_4 , using the formulae provided in Refs. [61,62]. However, rather than using the full ψ_4 we decompose it into ℓ and m modes and solve for the radiated linear momentum, dropping terms with $\ell \geq 5$. The formulae in Refs. [61,62] are valid at $r = \infty$. We obtain highly accurate values for these quantities by solving for them on spheres of finite radius (typically $r/M = 25, 30, 35, 40$), fitting the results to a polynomial dependence in $l = 1/r$, and extrapolating to $l = 0$. We perform

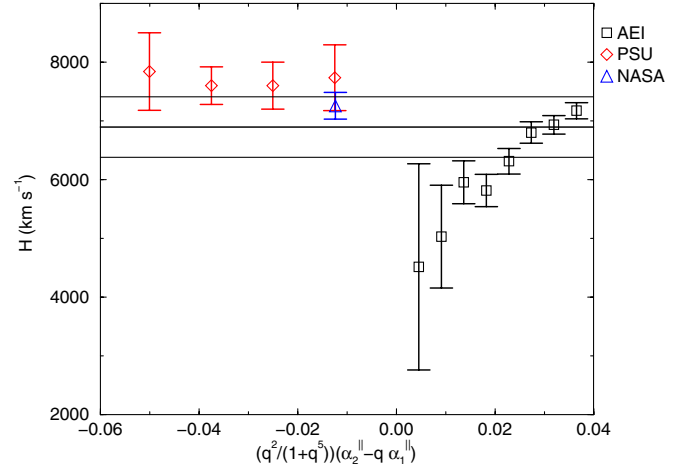


FIG. 1 (color online). The value of H calculated by inverting Eq. (2b) as determined from simulations by the AEI, PSU, and NASA/GSFC groups. The thick line is the weighted average and the thin lines are the expected uncertainty in the average.

fits based on a linear and quadratic dependence on l , and take the final values to be the average of these two extrapolations with the differences being the extrapolation error.

We obtain a new determination of H in Eq. (2b) using results from simulations performed by the NASA/GSFC [32], PSU [27], and AEI/LSU [41] groups. The simulations performed by these groups include runs with $q = 1$, and thus provide an accurate measurement of v_{\perp} . We calculate H for each simulation (via $H = v_{\perp}(\alpha_2^{\parallel} - \alpha_1^{\parallel})(1 + q)^5/q^2$) and take the weighted average $\langle H \rangle \pm \delta\langle H \rangle$, where

$$\langle X^n \rangle = \sum_i X_i^n w_i, \quad w_i = \frac{(\delta X_i)^{-2}}{\sum_j (\delta X_j)^{-2}}, \quad (7)$$

$$\delta\langle X \rangle = \sqrt{\langle X^2 \rangle - \langle X \rangle^2},$$

X is the quantity to be averaged, n is some specified power, and δX_i is the uncertainty in a particular measurement of X . Note that we weight H and H^2 by the same w_i . We find $\langle H \rangle = (6895 \pm 513) \text{ km s}^{-1}$. Figure 1 shows the values of H obtained from each simulation as well as the average value of H . We can see that based on the AEI/LSU data, which take into account the initial recoil at the beginning of the full numerical simulations, one could fit linear corrections to H . However, the deviations from $H = \text{const}$ are only significant near $D = q^2/(1 + q)^5(\alpha_2^{\parallel} - q\alpha_1^{\parallel}) = 0$, when the spin-induced recoil is small (and hence the relative error in the spin-induced recoil is large). The absolute differences between the predicted and measured recoil velocities for the AEI/LSU results are within 20 km s^{-1} when we take $H = 6895 \text{ km s}^{-1}$.

III. POST-NEWTONIAN ANALYSIS

In order to compare results from the recoil due to unequal masses and those due to spin effects as well, we

will study systems with similar orbital trajectories. Since the radiated momentum due to unequal masses is a function of the orbital acceleration, these systems will all exhibit very similar unequal-mass contributions to the net recoil, which allows us to isolate the spin-induced contributions to the recoil. To generate families of binaries with similar trajectories we use the formulae for the leading order post-Newtonian accelerations and choose configurations that minimize the effects of the spins on the trajectory,

but have non-negligible spin contributions to the net recoil.

The relative one-body accelerations can be written as [47]

$$\vec{a} = \vec{a}_N + \vec{a}_{\text{PN}} + \vec{a}_{2\text{PN}} + \vec{a}_{\text{RR}} + \vec{a}_{\text{SO}} + \vec{a}_{\text{SS}}, \quad (8)$$

with

$$\vec{a}_N = -\frac{m}{r^2} \hat{n}, \quad (9a)$$

$$\vec{a}_{\text{PN}} = -\frac{m}{r^2} \left\{ \hat{n} \left[(1 + 3\nu)v^2 - 2(2 + \nu)\frac{m}{r} - \frac{3}{2}\nu\dot{r}^2 \right] - 2(2 - \nu)\dot{r} \vec{v} \right\}, \quad (9b)$$

$$\begin{aligned} \vec{a}_{2\text{PN}} = & -\frac{m}{r^2} \left\{ \hat{n} \left[\frac{3}{4}(12 + 29\nu)\left(\frac{m}{r}\right)^2 + \nu(3 - 4\nu)v^4 + \frac{15}{8}\nu(1 - 3\nu)\dot{r}^4 - \frac{3}{2}\nu(3 - 4\nu)v^2\dot{r}^2 - \frac{1}{2}\nu(13 - 4\nu)\frac{m}{r}v^2 \right. \right. \\ & \left. \left. - (2 + 25\nu + 2\nu^2)\frac{m}{r}\dot{r}^2 \right] - \frac{1}{2}\dot{r} \vec{v} \left[\nu(15 + 4\nu)v^2 - (4 + 41\nu + 8\nu^2)\frac{m}{r} - 3\nu(3 + 2\nu)\dot{r}^2 \right] \right\}, \end{aligned} \quad (9c)$$

$$\vec{a}_{\text{RR}} = \frac{8}{5}\nu\frac{m^2}{r^3} \left\{ \dot{r} \hat{n} \left[18v^2 + \frac{2}{3}\frac{m}{r} - 25\dot{r}^2 \right] - \vec{v} \left[6v^2 - 2\frac{m}{r} - 15\dot{r}^2 \right] \right\}, \quad (9d)$$

$$\vec{a}_{\text{SO}} = \frac{1}{r^3} \left\{ 6\hat{n} \left[(\hat{n} \times \vec{v}) \cdot \left(2\vec{S} + \frac{\delta m}{m} \vec{\Delta} \right) \right] - \left[\vec{v} \times \left(7\vec{S} + 3\frac{\delta m}{m} \vec{\Delta} \right) \right] + 3\dot{r} \left[\hat{n} \times \left(3\vec{S} + \frac{\delta m}{m} \vec{\Delta} \right) \right] \right\}, \quad (9e)$$

$$\vec{a}_{\text{SS}} = -\frac{3}{\mu r^4} \left\{ \hat{n}(\vec{S}_1 \cdot \vec{S}_2) + \vec{S}_1(\hat{n} \cdot \vec{S}_2) + \vec{S}_2(\hat{n} \cdot \vec{S}_1) - 5\hat{n}(\hat{n} \cdot \vec{S}_1)(\hat{n} \cdot \vec{S}_2) \right\}, \quad (9f)$$

where $\vec{x} \equiv \vec{x}_1 - \vec{x}_2$, $\vec{v} = d\vec{x}/dt$, $\hat{n} \equiv \vec{x}/r$, $m = m_1 + m_2$, $\mu \equiv m_1 m_2 / m$, $\nu \equiv \mu/m$, $\delta m \equiv m_1 - m_2$, $\vec{S} \equiv \vec{S}_1 + \vec{S}_2$, and $\vec{\Delta} \equiv m(\vec{S}_2/m_2 - \vec{S}_1/m_1)$, and an overdot denotes d/dt .

The first four terms in Eq. (8) correspond to the Newtonian, first-post-Newtonian (1PN), second-post-Newtonian, and radiation reaction contributions to the equations of motion. The last two terms in Eq. (8) are the spin-orbit (SO) and spin-spin (SS) contributions to the acceleration.

The radiated linear momentum due to the motion of the two holes has the form [47]

$$\begin{aligned} \dot{\vec{P}}_N = & -\frac{8}{105} \frac{\delta m}{m} \nu^2 \left(\frac{m}{r}\right)^4 \left\{ \dot{r} \hat{n} \left[55v^2 - 45\dot{r}^2 + 12\frac{m}{r} \right] \right. \\ & \left. + \vec{v} \left[38\dot{r}^2 - 50v^2 - 8\frac{m}{r} \right] \right\}, \end{aligned} \quad (10)$$

plus higher post-Newtonian terms [63], while the radiated linear momentum due to spin-orbit effects has the form

$$\begin{aligned} \dot{\vec{P}}_{\text{SO}} = & -\frac{8}{15} \frac{\mu^2 m}{r^5} \{ 4\dot{r}(\vec{v} \times \vec{\Delta}) - 2v^2(\hat{n} \times \vec{\Delta}) \\ & - (\hat{n} \times \vec{v})[3\dot{r}(\hat{n} \cdot \vec{\Delta}) + 2(\vec{v} \cdot \vec{\Delta})] \}. \end{aligned} \quad (11)$$

Note also that the spin-spin coupling does not contribute to the radiated linear momentum to this order.

In order to best study and model how the final remnant recoil velocity depends on the mass ratio and spins, we will

choose configurations with black holes spinning along the orbital angular momentum. In this way the orbital plane will not precess and we can write [47]

$$\vec{S} = \vec{S}_1 + \vec{S}_2 = S^z \hat{z}, \quad (12)$$

and

$$\vec{v} = \dot{r} \hat{n} + r\omega \hat{\lambda}, \quad (13)$$

where $\vec{L}_N \equiv \mu(\vec{x} \times \vec{v})$ is the Newtonian orbital angular momentum, $\hat{\lambda} = \hat{L}_N \times \hat{n}$ with $\hat{L}_N = \vec{L}_N/|\vec{L}_N|$, and $\omega = d\phi/dt$ is defined as the orbital angular velocity.

Taking into account that the velocity remains in the orbital plane, i.e. Eq. (13), we find that the spin-orbit acceleration (9e) is given by

$$\vec{a}_{\text{SO}}^\perp = \frac{1}{r^3} \left\{ r\omega \left(5S^z + 3\frac{\delta m}{m} \Delta^z \right) \hat{n} - 2\dot{r} S^z \hat{\lambda} \right\}, \quad (14)$$

and the radiated linear momentum is given by

$$\dot{\vec{P}}_{\text{SO}}^\perp = \frac{16}{15} \frac{\mu^2 m \Delta^z}{r^5} \{ (\dot{r}^2 - r^2 \omega^2) \hat{\lambda} - 2\dot{r} r \omega \hat{n} \}, \quad (15)$$

and

$$\begin{aligned} \dot{\vec{P}}_N = & -\frac{8}{105} \frac{\delta m}{m} \nu^2 \left(\frac{m}{r}\right)^4 \left\{ \dot{r} \hat{n} \left[5r^2 \omega^2 - 2\dot{r}^2 + 4\frac{m}{r} \right] \right. \\ & \left. - r\omega \hat{\lambda} \left[50r^2 \omega^2 + 12\dot{r}^2 + 8\frac{m}{r} \right] \right\}. \end{aligned} \quad (16)$$

Note that if we take the scalar product of these two instantaneous radiated momenta we obtain

$$\begin{aligned} \dot{\vec{P}}_N \cdot \dot{\vec{P}}_{SO}^\perp / (\dot{P}_N \dot{P}_{SO}^\perp) &= \cos(\xi_{PN}^{\text{inst}}) \\ &= -\omega f(r, \dot{r}, \omega) / \sqrt{|g(r, \dot{r}, \omega)|}, \end{aligned} \quad (17)$$

where $f = 4r\dot{r}^4 + (8m + 24r^3\omega^2)\dot{r}^2 - r^2\omega^2(4m + 25r^3\omega^2)$ and $g(r, \dot{r}, \omega) = 4\dot{r}^6 - (16m - 124r^3\omega^2 - r)\dot{r}^4/r + (16m^2 + 232r^3\omega^2m + 1225r^6\omega^4 + 2r^4\omega^2)\dot{r}^2/r^2 + \omega^2(64m^2 + 800r^3\omega^2m + 2500r^6\omega^4 + r^4\omega^2)$. The fact that the factor of Δ^z drops out of Eq. (17) suggests that ξ (which is the angle between the cumulative radiated linear momenta) will depend only weakly on the spins through their effects on the orbital motion. Binaries with similar orbital trajectories should therefore have similar values for ξ . Note that ξ may still be a strong function of trajectory and q .

We will now turn to the question of identifying a subset of physical parameters of the binary that produce similar trajectories for unequal-mass, nonspinning and unequal-mass, spinning binaries in order to compare their recoil velocities and extract the spin contribution to the total recoil.

A. Similar radial trajectories

An analysis of how ξ depends on configuration is greatly simplified if the trajectories of the spinning binaries are similar to the trajectory for a nonspinning binary with the same mass ratio. In order to accomplish this, we use the post-Newtonian expression for the spin-orbit induced acceleration Eq. (14), and choose a configuration that minimizes its effect.

The radial component of the spin-orbit induced acceleration will vanish if $5S^z + 3\frac{\partial m}{m}\Delta^z = 0$. This leads to the condition

$$F = (3q + 2) + (3 + 2q)\tilde{\alpha} = 0, \quad (18)$$

where $\tilde{\alpha} = q\alpha_1/\alpha_2$ can take any positive or negative value. However, if we consider the algebraic average over the range $0 \leq q \leq 1$ at fixed F we find

$$\langle \tilde{\alpha} \rangle = \frac{1}{2}[\tilde{\alpha}(q=0) + \tilde{\alpha}(q=1)] = \frac{4}{15}F - \frac{5}{6} \quad (19)$$

and that $\tilde{\alpha} = \langle \tilde{\alpha} \rangle$ when $q = 3/8$ (independent of F).

We will thus study configurations with this mass ratio (which also produces a nearly maximum recoil velocity of $\approx 175 \text{ km s}^{-1}$ for nonspinning unequal-mass black-hole binaries [23]).

Hence the first family of black-hole-binary configurations that we will study is given by the choice

$$F = 0, \quad q = 3/8, \quad (20)$$

thus

$$\alpha_2/\alpha_1 = -q(3 + 2q)/(2 + 3q) = -9/20. \quad (21)$$

The total spin of the binary will in general be nonvanishing with

$$S^z/m^2 = (\alpha_2 + q^2\alpha_1)/(1 + q)^2 = 4\alpha_2/11. \quad (22)$$

B. Similar tangential trajectories

We can also choose a configuration where the tangential component of the acceleration due to the spin-orbit coupling vanishes, i.e.

$$S^z = S_1^z + S_2^z = 0. \quad (23)$$

This translates into the condition

$$\alpha_2/\alpha_1 = -q^2 = -9/64 \quad (24)$$

when $q = 3/8$. Note that now, the radial acceleration, as parametrized by F , is nonvanishing

$$F = (3q + 2) + (3 + 2q)q\alpha_1/\alpha_2 = -55/8. \quad (25)$$

Thus, for $q \neq 1$, we cannot make both the radial and tangential components of the spin-orbit acceleration vanish at the same time by a simple choice of physical parameters of the binary.

IV. INITIAL CONFIGURATIONS

We choose quasicircular initial configurations with mass ratio $q = m_1/m_2 = 3/8$ from four families of parameters that we will denote by Q , F , S , and A . The Q -series has initially nonspinning holes, the F -series has $F = 0$ (see Eq. (18)); hence zero PN spin-orbit-induced radial acceleration, the S -series has total spin $\vec{S} = 0$; hence zero PN spin-orbit-induced tangential acceleration, and the A -series has neither $F = 0$ nor $S = 0$; hence both spin-orbit-induced accelerations are nonvanishing. The puncture masses were fixed by requiring that the total Arnowitt-Deser-Misner (ADM) mass of the system be 1 and that the mass ratio of the horizon masses be $3/8$. The initial data parameters for these configurations are given in Tables I and II. We obtained initial data parameters by choosing spin and linear momenta consistent with 3PN quasicircular orbits for binaries with mass ratio $q = 3/8$ and then solve for the Bowen-York ansatz for the initial 3-metric and extrinsic curvature. This method was pioneered by the Lazarus project [64] (see Fig. 35 there), and then used in the rest of the breakthrough papers [6–8,39,48,62] by the authors (in Ref. [28] we used the PN expressions for the radial component of the momentum as well).

V. RESULTS

We evolved all configurations given in Tables I and II using 10 levels of refinement with a finest resolution of $h = M/80$ and outer boundaries at $320M$ except configuration $A_{+0.9}$, where we used an additional coarse level to push the outer boundaries to $640M$. In all cases, except

TABLE I. Initial data parameters for quasicircular orbits with orbital frequency $\omega/M = 0.05$. All sets have mass ratio $q = m_1^H/m_2^H = 3/8$. The “F” series has $\alpha = \alpha_2/\alpha_1 = -9/20$ (hence $F = q\alpha_1/\alpha_2(2q + 3) + 3q + 2 = 0$), and the “S” series has $\tilde{S} = \tilde{S}_1 + \tilde{S}_2 = 0$. The punctures are located along the x -axis with momenta $\vec{P}_1 = (0, P, 0)$ and $\vec{P}_2 = (0, -P, 0)$, and spins \vec{S}_i along the z -axis. m_i^p are the puncture masses, m_i^H are the horizon masses.

Config.	Q_{38}	$F_{+0.2}$	$F_{-0.2}$	$F_{+0.4}$	$F_{-0.4}$	$S_{+0.64}$	$S_{-0.64}$
x_1/M	-4.745 565 2	-4.688 932 9	-4.800 884 7	-4.631 031 2	-4.854 840 1	-4.531 023 5	-4.956 139 2
x_2/M	1.760 457 2	1.816 103 7	1.704 274 0	1.871 165 0	1.647 599 3	1.897 592	1.616 822 4
S_1^z/M^2	0.000 000 0	0.015 219 622	-0.015 222 140	0.030 437 161	-0.030 447 242	0.048 726 127	-0.048 689 700
S_2^z/M^2	0.000 000 0	-0.048 702 791	0.048 710 847	-0.097 398 914	0.097 431 175	-0.048 726 127	0.048 689 700
P/M	0.106 821 12	0.107 079 29	0.106 567 47	0.107 342 44	0.106 317 92	0.106 763 49	0.106 929 58
L^z/M^2	0.694 980 63	0.696 554 681 6	0.693 238 274 4	0.697 961 617 8	0.691 325 865 8	0.686 341 552 4	0.702 844 019 6
J/M^2	0.694 980 63	0.663 071 512 9	0.726 726 981 9	0.630 999 864 3	0.758 309 798 7	0.686 341 552 4	0.702 844 019 6
m_1^p/M	0.257 487 828	0.253 193 14	0.253 279 647	0.239 665 153	0.239 816 706	0.205 915 971	0.206 131 153
m_2^p/M	0.718 534 208	0.716 211 70	0.716 211 394	0.709 030 409	0.709 034 88	0.715 832 591	0.715 746 409
m_1^H/M	0.275 829 74	0.275 778 86	0.275 791 869	0.275 757 065	0.275 775 78	0.275 695 9	0.275 581 21
m_2^H/M	0.735 411 00	0.735 414 02	0.735 444 371	0.735 334 919	0.735 402 505	0.735 186 1	0.734 888 095
α_1^z	0.000	0.200 125 82	-0.200 138 25	0.400 298 251 6	-0.400 383 662	0.641 176 6	-0.641 190 84
α_2^z	0.000	-0.090 053 523	0.090 061 911 9	-0.180 130 779	0.180 158 74	-0.090 153	0.090 158 83
M_{ADM}/M	1.000 01	1.000 01	0.999 997	1.000 01	0.999 997	1.000 01	0.999 991

where noted otherwise, we set the free Gamma-driver parameter in Eq. (3c) to $\eta = 6/M$ [2,57].

In a generic simulation both the unequal mass and spin components of the recoil are functions of the trajectory. To single out each individual effect we perform runs chosen to follow similar trajectories. In order to compare recoil velocity directions between these runs we need to rotate each system so that the final plunge (where most of the recoil is generated) occurs along the same direction. We do this in two ways. First, as demonstrated in Fig. 2, we plot

TABLE II. Initial data parameters for quasicircular orbits with orbital frequency $\omega/M = 0.05$. All sets have mass ratio $q = m_1^H/m_2^H = 3/8$. The punctures are located along the x -axis with momenta $\vec{P}_1 = (0, P, 0)$ and $\vec{P}_2 = (0, -P, 0)$, and spins \vec{S}_i along the z -axis. m_i^p are the puncture masses, m_i^H are the horizon masses. In this series neither F nor S vanishes.

Config.	$A_{+0.9}$	$A_{-0.9}$
x_1/M	-4.544 343 8	-4.866 256 3
x_2/M	1.573 114	1.927 519 2
S_1^z/M^2	0.000 000 0	0.000 000 0
S_2^z/M^2	0.488 737 79	-0.485 816 09
P/M	0.102 764 65	0.110 893 09
L^z/M^2	0.628 658 477	0.753 382 740
J/M^2	1.117 396 265	0.267 566 654
m_1^p/M	0.254 566 6	0.254 580 6
m_2^p/M	0.282 229 9	0.284 150 275
m_1^H/M	0.273 356 4	0.272 629 2
m_2^H/M	0.728 824	0.727 009 3
α_1^z	0.000 000 0	0.000 00
α_2^z	0.920 196 524	-0.919 212 1
M_{ADM}/M	1.000 000	0.999 991

the puncture trajectory difference $\vec{r} = \vec{r}_1 - \vec{r}_2$ (where $\vec{r}_i(t)$ is the coordinate location of puncture i at time t) for each case and rotate the trajectories by an angle Φ_{track} so that they all line up with the Q_{38} trajectory during the late-inspiral and merger phases. Note that by taking the differences between trajectories we remove effects due to the wobble motion of the center of mass. Second, we measure the phase of the dominant ($\ell = 2, m = 2$) mode of ψ_4 at the point of peak amplitude and take half the phase difference between each case and Q_{38} (since ψ_4 has spin-weight -2 , a rotation of ϕ about the z -axis will introduce a phase difference of -2ϕ in ψ_4). We denote this latter rotation angle by Φ_{ψ_4} . We get reasonable agreement between these two measures of the rotation angle (see Table III). This type of rotation may also be needed when comparing results from different resolutions of the same configuration (i.e. when the phase error, but not the amplitude error, is large). In Table IV we give the components of the recoil velocity for a set of Q_{38} simulations with $\eta = 2/M$. This value of η leads to a poorer effective resolution than for our standard choice of $\eta = 6/M$. Consequently there is a relatively large phase error in the low resolution results. After performing the rotation, the recoil velocities agree to within errors.

Note that there is no rotation which will make the $A_{+0.9}$ or $A_{-0.9}$ trajectories line up with the Q_{38} trajectory. In these cases the hang-up effect [6] due to spin-orbit coupling significantly alters the trajectories (see Fig. 3).

Once we have found the correct rotation angle we obtain ξ via

$$\begin{aligned} \vec{V}_{\text{recoil}} &= R[\Phi]\vec{V}_{\text{recoil}}, & \vec{V}_{\text{spin}} &= \vec{V}_{\text{recoil}} - \vec{V}_{Q38}, \\ \cos(\xi) &= \vec{V}_{\text{spin}} \cdot \hat{V}_{Q38}, \end{aligned} \quad (26)$$

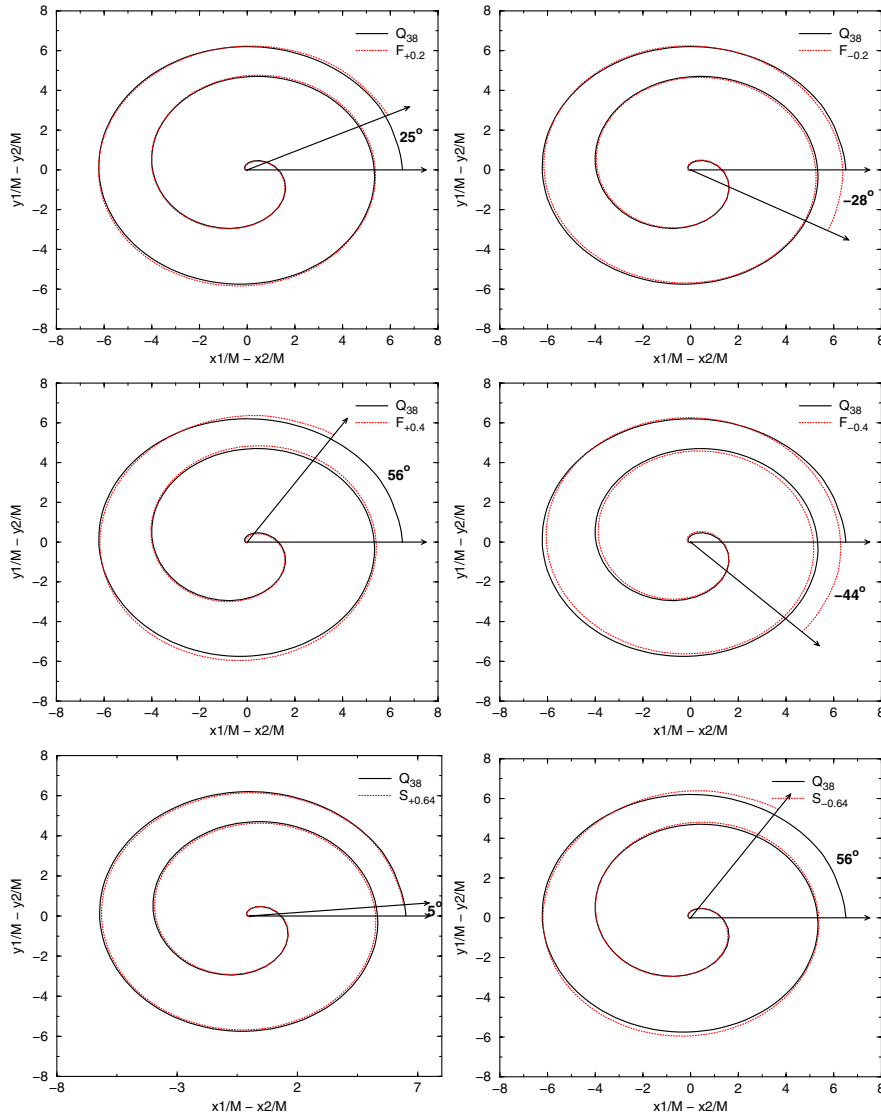


FIG. 2 (color online). The trajectory differences $\vec{r} = \vec{r}_1 - \vec{r}_2$ for the “F” and “S” series rotated so that the late-inspiral matches the Q_{38} trajectory. The plots show the rotation angle Φ_{track} .

TABLE III. The rotation angle needed to align the trajectories of each simulation with the Q_{38} simulation as measured directly from the orbital trajectories (Φ_{track}) and using the phase of the waveform at the point of maximum amplitude (Φ_{ψ_4}). Note that Φ_{ψ_4} provides the rotation angle modulo 180° .

Config.	Φ_{track}	Φ_{ψ_4}	$ \Phi_{\text{track}} - \Phi_{\psi_4} $
F _{+0.2}	25°	34.5°	9.5°
F _{-0.2}	-28°	-35.5°	7.5°
F _{+0.4}	56°	63.1°	7.1°
F _{-0.4}	-44°	-40.0°	4.0°
S _{+0.64}	5°	9.7°	4.7°
S _{-0.64}	56°	44.6°	11.4°
A _{+0.9}	***	12.3°	***
A _{-0.9}	***	-15.9°	***

TABLE IV. Results of the recoil velocity for the Q_{38} configuration with $\eta = 2/M$ at two different resolutions. After correcting for the phase error, equivalent to a rotation, the two recoils agree. Here “ R_{track} ” denotes the velocity after rotating by the angle Φ_{track} and “ R_{ψ_4} ” denotes the velocity after rotating by the angle Φ_{ψ_4} .

h	Φ_{track}	Φ_{ψ_4}	V_x	V_y
$M/80$	34°	36.5°	-163 ± 12	-46 ± 11
$M/80R_{\psi_4}$	***	***	-103 ± 12	-134 ± 11
$M/80R_{\text{track}}$	***	***	-109 ± 12	-129 ± 11
$M/100$	0	0	-109 ± 14	-133 ± 12

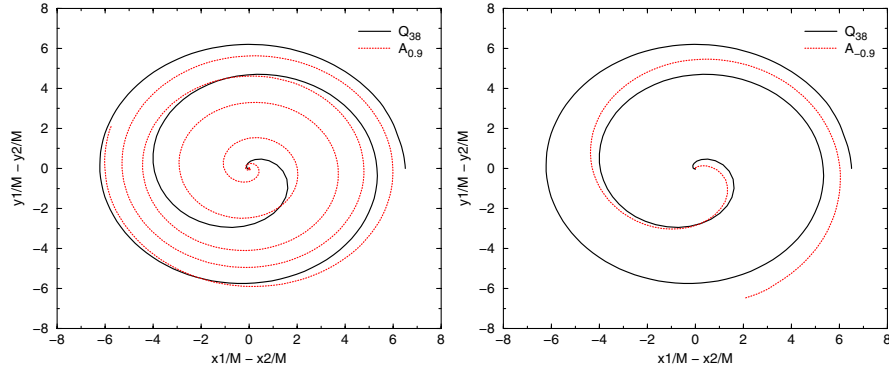


FIG. 3 (color online). The trajectory differences $\vec{r} = \vec{r}_1 - \vec{r}_2$ for the “A” series, as well as Q_{38} . Note that there is no angle Φ_{track} that will make the late-time trajectories overlap. Here the spin-orbit hang-up effect changes the orbital trajectory significantly.

where \vec{V}_{recoil} is the measured recoil velocity, $R[\Phi]$ rotates \vec{V}_{recoil} by an angle Φ in the xy plane, and $\vec{V}_{Q_{38}}$ is the recoil of the Q_{38} configuration. Note that when $\alpha_2^{\parallel} - q\alpha_1^{\parallel} < 0$ we need to replace ξ by $\pi - \xi$ in formula (26) since the coefficient v_{\perp} in Eq. (1) is negative. We calculate two different values of ξ , ξ_{track} , and ξ_{ψ_4} , based on the rotation angles Φ_{track} and Φ_{ψ_4} , respectively. We obtain an additional measurement of ξ by solving for $\cos\xi$ using Eq. (1) and the measured values of the recoil magnitude. We denote this latter measurement of ξ , which is unaffected by rotations, by ξ_{Formula} , where

$$\xi_{\text{Formula}} = \cos^{-1} \left[\frac{v^2 - v_m(q)^2 - v_{\perp}(q, \alpha_1^{\parallel}, \alpha_2^{\parallel})^2}{2v_m(q)v_{\perp}(q, \alpha_1^{\parallel}, \alpha_2^{\parallel})} \right], \quad (27)$$

v_m is given by Eq. (2a), v_{\perp} is given by Eq. (2b), and v is the measured magnitude of the recoil velocity.

We summarize the results of our simulations in Tables V and VI. All configurations, with the exception of the “A” series, have radiated energies in the range $E_{\text{rad}}/M = 0.021 \pm 0.002$ and radiated angular momenta in the range $J_{\text{rad}}/M^2 = 0.15 \pm 0.01$, which is consistent with these trajectories being essentially the same for all configurations (see Fig. 2).

We obtain weighted averages for ξ for the “F” and “S” series of $\langle \xi_{\text{track}} \rangle = (152 \pm 9)^{\circ}$, $\langle \xi_{\psi_4} \rangle = (143 \pm 14)^{\circ}$, and $\langle \xi_{\text{Formula}} \rangle = (144 \pm 7)^{\circ}$, where we use Eq. (7) to obtain the weighted average and uncertainty. These weighted averages are consistent with the measured values of ξ . The weighted average over all three measurements of ξ is $\langle \xi \rangle = (145 \pm 10)^{\circ}$. Interestingly, $\langle \xi \rangle$ provides an accurate prediction for the recoil velocity of the $A_{-0.9}$ configuration. This result is unexpected because the recoil due to unequal masses is a function of the mass ratio and the trajectories

TABLE V. The recoil velocities (prior to any rotation), radiated energy, and angular momentum, and ξ for the “Q” and “F” series. ξ_{track} is calculated using Φ_{track} and Eq. (26), ξ_{ψ_4} is calculated using Φ_{ψ_4} and Eq. (26), ξ_{Formula} is calculated from the given recoil magnitude using Eq. (27). $|\vec{V}_{\text{track}}^{\text{pred}}|$, $|\vec{V}_{\psi_4}^{\text{pred}}|$, and $|\vec{V}_{\text{avg}}^{\text{pred}}|$ are the recoil velocities as predicted by Eq. (1) with $\xi = \xi_{\text{track}}$, $\xi = \xi_{\psi_4}$, and $\xi = \langle \xi \rangle$, respectively.

Config.	Q_{38}	$F_{+0.2}$	$F_{-0.2}$	$F_{+0.4}$	$F_{-0.4}$
E_{rad}/M	0.0210 ± 0.0003	0.0202 ± 0.0003	0.0219 ± 0.0004	0.0193 ± 0.0002	0.0228 ± 0.0004
J_{rad}/M^2	0.1503 ± 0.0030	0.1471 ± 0.0005	0.1576 ± 0.0015	0.1399 ± 0.0016	0.1625 ± 0.0010
V^x [km s $^{-1}$]	-94 ± 11	-177 ± 10	-15 ± 14	-223 ± 12	15 ± 14
V^y [km s $^{-1}$]	-141 ± 5	-85 ± 12	-155 ± 5	33 ± 18	-127 ± 4
$ \vec{V} $ [km s $^{-1}$]	169.5 ± 7.4	196.4 ± 10.4	155.7 ± 7.2	225.4 ± 12.2	127.9 ± 4.3
ξ_{track} [deg]	0°	$(143 \pm 31)^{\circ}$	$(178 \pm 73)^{\circ}$	$(147 \pm 20)^{\circ}$	$(169 \pm 21)^{\circ}$
ξ_{ψ_4} [deg]	0°	$(154 \pm 43)^{\circ}$	$(127 \pm 41)^{\circ}$	$(173 \pm 25)^{\circ}$	$(179 \pm 21)^{\circ}$
ξ_{Formula} [deg]	0°	$(127 \pm 26)^{\circ}$	$(131 \pm 15)^{\circ}$	$(134 \pm 20)^{\circ}$	$(144 \pm 6)^{\circ}$
$ \vec{V}_{\text{track}}^{\text{pred}} $ [km s $^{-1}$]	175	202 ± 9	142 ± 3	232 ± 10	112 ± 9
$ \vec{V}_{\psi_4}^{\text{pred}} $ [km s $^{-1}$]	175	205 ± 9	158 ± 21	240 ± 5	110 ± 5
$ \vec{V}_{\text{avg}}^{\text{pred}} $ [km s $^{-1}$]	175	203 ± 3	150 ± 4	231 ± 5	127 ± 8

TABLE VI. The recoil velocities (prior to any rotation), radiated energy, and angular momentum, and ξ for the “S” and “A” series. Note that although we report the calculated values for ξ based on Φ_{ψ_4} for the “A” series, here ξ is not well defined because the unequal-mass component of the recoil is not given by the Q_{38} recoil. ξ_{track} is calculated using Φ_{track} and Eq. (26), ξ_{ψ_4} is calculated using Φ_{ψ_4} and Eq. (26), ξ_{Formula} is calculated from the given recoil magnitude using Eq. (27). $|\vec{V}_{\text{track}}^{\text{pred}}|$, $|\vec{V}_{\psi_4}^{\text{pred}}|$, and $|\vec{V}_{\text{avg}}^{\text{pred}}|$ are the recoil velocities as predicted by Eq. (1) with $\xi = \xi_{\text{track}}$, $\xi = \xi_{\psi_4}$, and $\xi = \langle \xi \rangle$, respectively.

Config.	$S_{0+0.64}$	$S_{-0.64}$	$A_{+0.9}$	$A_{-0.9}$
E_{rad}/M	0.0209 ± 0.0003	0.0203 ± 0.0002	0.050668 ± 0.000974	0.01274 ± 0.00003
J_{rad}/M^2	0.152 ± 0.0007	0.146 ± 0.001	0.2999857 ± 0.00708	0.092 ± 0.001
$V^x[\text{km s}^{-1}]$	-122 ± 18	-119 ± 5	13 ± 30	48 ± 24
$V^y[\text{km s}^{-1}]$	-181 ± 15	31 ± 4	-63 ± 2	-340 ± 8
$ \vec{V} [\text{km s}^{-1}]$	218.3 ± 16.0	123.0 ± 4.9	64.1 ± 5.9	343.4 ± 8.6
$\xi_{\text{track}}[\text{deg}]$	$(160 \pm 31)^\circ$	$(148 \pm 11)^\circ$	***	***
$\xi_{\psi_4}[\text{deg}]$	$(142 \pm 28)^\circ$	$(137 \pm 7)^\circ$	$(158 \pm 7)^\circ$	$(93 \pm 7)^\circ$
$\xi_{\text{Formula}}[\text{deg}]$	$(124 \pm 22)^\circ$	$(150 \pm 7)^\circ$	$(159 \pm 2)^\circ$	$(149 \pm 19)^\circ$
$ \vec{V}_{\text{track}}^{\text{pred}} [\text{km s}^{-1}]$	237 ± 10	125 ± 10	***	***
$ \vec{V}_{\psi_4}^{\text{pred}} [\text{km s}^{-1}]$	230 ± 16	135 ± 7	68 ± 22	259 ± 18
$ \vec{V}_{\text{avg}}^{\text{pred}} [\text{km s}^{-1}]$	231 ± 5	127 ± 8	108 ± 28	340 ± 9

(i.e. the accelerations of the masses over time). For the “F” and “S” configurations the trajectories are very similar to Q_{38} , and hence the unequal-mass components of the recoil are expected to be very similar to Q_{38} . However, the spin-orbit coupling induced hang-up effect in both $A_{+0.9}$ and $A_{-0.9}$ greatly affects the trajectories (see Fig. 3), as well as the radiated energy and angular momenta. If we consider the radiated linear momentum averaged over an orbit, then we see that the slower the inspiral (i.e. the closer to a closed orbit), the smaller the average recoil. Hence we expect that $A_{+0.9}$ will have a smaller unequal-mass recoil than Q_{38} , while $A_{-0.9}$ will have a larger one. To quantify how much the orbits close we take the average of $\vec{r} = \vec{r}_1 - \vec{r}_2$ over the trajectory from the beginning of each simulation until $|\vec{r}| \sim 0.1$. The resulting averages $|\langle \vec{r} \rangle|$ for the “Q,” “F,” “S,” and “A” families are given in Table VII. The mean and standard deviation of $|\langle \vec{r} \rangle|$ for the “Q,” “F,” and “S” configurations is $|\langle \vec{r} \rangle| = 0.865 \pm 0.070$. The $A_{+0.9}$ and $A_{-0.9}$ configuration lie 7.1σ and 7.6σ below and above this mean, respectively, while the results for the other configurations lie within 1.4σ of the mean.

As seen in Fig. 4 the angle ξ appears, at least qualitatively, to be independent of Δ . This is in agreement with our post-Newtonian analysis in Eq. (17). It is also consistent with our intuition that similar trajectories imply simi-

lar angles between the unequal-mass and spin contributions to the recoil, and it seems that the small differences in the trajectories produce some scatter on the values, but this is apparently mostly due to the numerical error generated during the simulations. It would be interesting to use this value of ξ to model the recoil velocity distribution in galaxies.

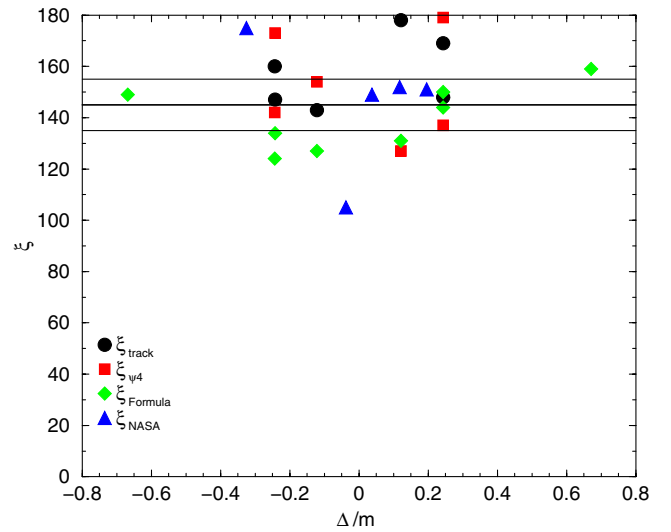


FIG. 4 (color online). ξ versus $\Delta/m = S_2/m_2 - S_1/m_1$ as calculated in this work for a mass ratio $q = 3/8$ and from the data published by the NASA/GSFC group for a mass ratio $q = 2/3$ provided in Ref. [32]. We plot ξ_{track} , ξ_{ψ_4} , and ξ_{Formula} for the “F” and “S” configurations and ξ_{Formula} for “A” configurations. The thick horizontal line and the two thin horizontal lines show the average value $\langle \xi \rangle$ and its uncertainty (as calculated in this work from our simulations). The data displays significant scatter, but appears to be consistent with $\xi = \text{const}$.

TABLE VII. The average value $|\langle \vec{r} \rangle|$ of the trajectories for each configuration. The larger the value of $|\langle \vec{r} \rangle|$ the slower the inspiral.

Config.	$ \langle \vec{r} \rangle $	Config.	$ \langle \vec{r} \rangle $	Config.	$ \langle \vec{r} \rangle $
Q_{38}	0.858 303	$F_{+0.2}$	0.902 234	$F_{-0.2}$	0.798 215 7
$F_{+0.4}$	0.936 172	$F_{-0.4}$	0.767 45	$S_{+0.64}$	0.845 197
$S_{-0.64}$	0.953 33	$A_{+0.9}$	0.365 654	$A_{-0.9}$	1.398 69

VI. GENERIC EVOLUTION REANALYZED

In light of our new understanding about the modeling of the recoil velocity, we reexamine our original generic binary configuration, which we denote by SP6. The SP6 configuration has a mass ratio of $q = 1/2$ with the larger hole having specific-spin $a/m = 0.885$ and spin pointing 45° below the orbital plane, and the smaller hole having negligible spin. We also evolved a similar configuration, which we will denote by SP6R, that is identical to SP6, but with the spin rotated by 90° about the z -axis. We evolved both configurations using the same grid structure as in the previous section, but used $\eta = 2/M$ rather than $6/M$. This choice of smaller η has the effect of reducing the effective resolution, but makes calculations of the quasilocal linear momentum and spin direction more accurate (see Ref. [39]) by reducing coordinate distortions. The initial data parameters for the two configurations are given in Table VIII. The drop in effective resolution when reducing η from $6/M$ to $2/M$ is significant. In our simulations we found that a Q_{38} , $\eta = 2/M$ run with central resolution of $M/100$ had a slightly larger waveform phase error than an equivalent $M/80$ resolution run with $\eta = 6/M$, while an $M/80$ run with $\eta = 2/M$ displayed a significant phase error. We have found in general that, with our choice of gauge, the coordinate dependent measurements, such as spin and linear momentum direction, become more accurate as η is reduced (and $h \rightarrow 0$). However, if η is too small ($\eta \lesssim 1/M$), the runs may become unstable. Similarly, if η is too large ($\eta \gtrsim 10/M$), then grid stretching effects can cause the remnant horizon to continuously grow, eventually leading to an unacceptable loss in accuracy at late times. We have found that a value of $\eta = 6/M$ provides both very high accuracy in the computed waveform at modest resolutions, while keeping the remnant horizon size nearly fixed at late times.

We measure a net recoil of $V_{\text{recoil}} = 375 \pm 18 \text{ km s}^{-1}$ and $V_{\text{recoil}} = 848 \pm 20 \text{ km s}^{-1}$ for SP6 and SP6R, respectively.

The analysis of the recoil in SP6 and SP6R is complicated by the fact that the orbital plane precesses significantly during the merger. Thus, we cannot associate the xy components of the recoil with the in-plane recoil (as was done tentatively in Ref. [28]). In order to measure the

TABLE VIII. Initial data parameters for the SP6 and SP6R configurations. m_p is the puncture mass parameter of the two holes. SP6 has spins $\vec{S}_1 = (0, S, -S)$ and $\vec{S}_2 = (0, 0, 0)$, momenta $\vec{P} = \pm(P_r, P_\perp, 0)$, puncture positions $\vec{x}_1 = (x_+, d, d)$ and $\vec{x}_2 = (x_-, d, d)$, masses m_1 and m_2 , and $M_{\text{ADM}}/M = 1.00000 \pm 0.00001$. SP6R has the same parameters as SP6 with the exception that $\vec{S}_1 = (-S, 0, -S)$.

m_p/M	0.3185	d/M	0.0012817	m_1/M	0.6680
x_+/M	2.68773	P_r/M	-0.0013947	m_2/M	0.3355
x_-/M	-5.20295	P_\perp/M	0.10695	S/M^2	0.27941

precession of the orbital plane we need an accurate measurement of the orbital angular momentum. Here we use the approximate formula

$$\vec{L}_{\text{orbit}} = \sum_i \vec{r}_i \times \vec{P}_i, \quad (28)$$

where \vec{r}_i is the coordinate location of puncture i and \vec{P}_i is the quasilocal momentum [39], given by Eq. (6), of black hole i . In Fig. 5 we show the orbital angular momentum of the SP6 configuration versus time. Note the rapid change in direction near merger (a common horizon was first detected at $t = 207.4M$), and as seen in Fig. 6, most of the recoil is generated about $3M$ to $30M$ after merger (here we assume that waveform features seen at $t = \tau$ for an observer at $r = 40M$ were generated by dynamics near the horizons at $t \sim \tau - 40M$). This rapid change in direction has a strong effect on the computed recoil due to the $\cos\Theta$ and $\cos\xi$ dependence of v_{recoil} . That is, rapid physical changes in the orbital plane and spin direction lead to relatively large errors in the direction (but not magnitude) of both the spin and orbital angular momenta when the resolution is below some threshold. This in turn leads to relatively large errors in the measured recoil. Thus it is not surprising that this new calculation of the recoil velocity for SP6 is 100 km s^{-1} smaller than the value we reported in [28] (note that we used a higher effective resolution in [28], thus we expect those values to be more accurate). These large errors will not be observed in more symmetric binaries where either the spin or angular momentum axes are fixed.

We can obtain an approximate measurement of α_{\parallel} and α_{\perp} using Eq. (28) and the measured direction of the spin. This estimation is only approximate due to the coordinate dependent nature of both calculations. We find that for

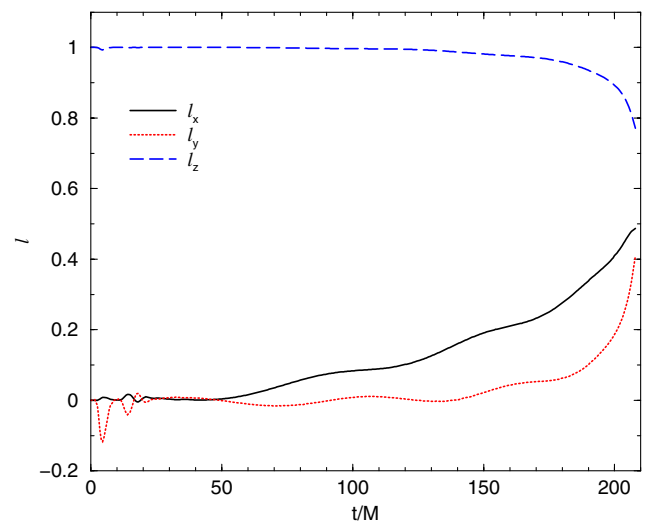


FIG. 5 (color online). The normalized orbital angular momentum vector $\vec{\ell} = \vec{L}/|\vec{L}|$ versus time for the SP6 configuration up to merger. Note the rapid change in the direction at late times.

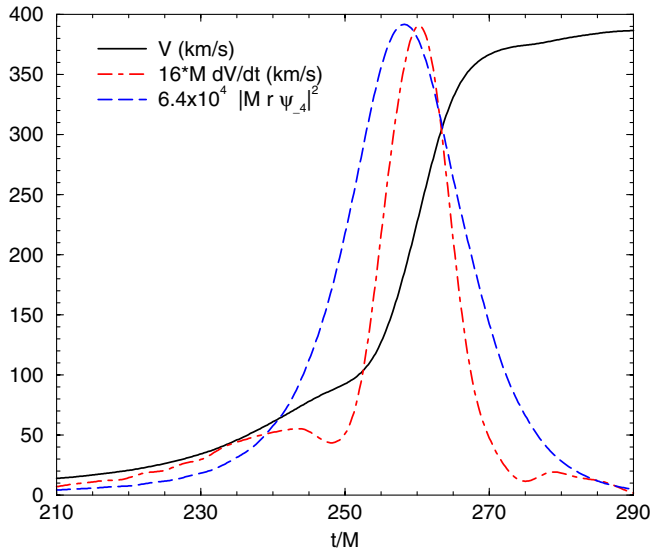


FIG. 6 (color online). The recoil speed ($V = |\vec{V}|$) for the SP6 configuration as measured from ψ_4 at $r = 40M$ as a function of time, as well as the time derivative of the recoil speed ($dV/dt = \hat{V} \cdot \dot{\vec{V}}$), and the magnitude of ψ_4 . Here the initial data burst is excluded from the calculation. Note that peak in dV/dt is located between $t = 250M$ and $t = 270M$ and occurs about $2M$ later than the peak in $|\psi_4|$. A common horizon was first detected at $t = 207.4M$, strongly suggesting that most of the recoil velocity is built up around merger time (since the observer is at $r = 40M$, features in the waveform at time $t = \tau$ originated near the horizon(s) at time $t \sim \tau - 40M$).

SP6, α_{\parallel} and α_{\perp} vary little over the course of the run with values at merger of $\alpha_{\parallel} = -0.62 \pm 0.03$ and $\alpha_{\perp} = 0.62 \pm 0.03$ (which are within errors of the initial values). However, the SP6R configuration does show a definite change in α over time, with merger values of $\alpha_{\parallel} = -0.69 \pm 0.03$ and $\alpha_{\perp} = 0.54 \pm 0.03$. We can use Eq. (1) to give estimates for the predicted recoil velocity if we make the following assumptions: (1) $\xi = \langle \xi \rangle$, (2) Θ for SP6R is rotated by $\pi/2$ radians with respect to SP6, and (3) Θ_0 is the same for SP6 and SP6R. Given these assumptions and the above range of the values for α_{\parallel} and α_{\perp} , we can perform a nonlinear least-squares fit of the recoil magnitude for SP6 and SP6R to obtain Θ_0 . The resulting predictions for the recoil magnitude are $V_{\text{SP6}} = (500 \pm 60) \text{ km s}^{-1}$ and $V_{\text{SP6R}} = (1120 \pm 130) \text{ km s}^{-1}$. Both predictions are within 2σ of the actual measured values and have an absolute error of 32%. If we fix α_{\parallel} and α_{\perp} to their average values and vary our guess for ξ over the range $(0, 360^\circ)$, we find that the predicted values for V_{SP6} and V_{SP6R} lie in the ranges $(462, 495) \text{ km s}^{-1}$ and $(1048, 1120) \text{ km s}^{-1}$, respectively.

The SP6 configuration demonstrated that the in-plane component of the spin can be the dominant contribution to the recoil. Given this observation, it becomes very important to accurately model this recoil. In Appendix A we derive a post-Newtonian model for the recoil produced by

this in-plane component and show that it predicts the $\cos\Theta$ dependence in our empirical formula.

VII. DISCUSSION

Interestingly, most of the recoil velocity imparted to the remnant is generated at around merger time (more precisely, as seen in Fig. 6, within the first few tens of M after merger. See also Refs. [21,28,37]), a nonlinear regime where post-Newtonian approximations are not expected to work, but where the ‘‘Lazarus’’ approach [64–69] can be successfully applied [19].

Although an accurate modeling of ξ is challenging, starting from an ansatz that $\xi = \xi(q, \Delta)$, we have found that, for quasicircular orbits, ξ is qualitatively independent of either Δ or q for $q = 3/8$, $q = 2/3$ (based on the results of Ref. [32]), and $q = 1/2$ (based on SP6). Note that the ξ that we measure is consistent with a similar parameter introduced in Ref. [32], where they found $\xi = 147^\circ$ (in our notation), based on a least-squares fit of the magnitude of the recoil versus a simplified version of Eq. (1). We know from the results for head-on collision (where $\xi = \pi/2$), that ξ is a function of eccentricity. However, for quasicircular orbits, it appears to vary only marginally with either q or Δ . Further long-term simulations with high accuracy (including extrapolations to $h \rightarrow 0$ and $\eta \rightarrow 0$) and further separated binaries will be needed in order to obtain a highly accurate model for ξ . In particular, the $\eta \rightarrow 0$ limit will be important because the recoil depends sensitively on the linear momenta and spin directions of the individual black holes near merger (where gauge effects are most severe), and hence we need to take the $\eta \rightarrow 0$ limit in order to accurately measure \vec{a} , \vec{L} , and Θ . Nevertheless, our simple formula holds with enough accuracy for astrophysical applications. In particular we have seen that the determination of an average value for the angle ξ of 145° seems to work not only for the F and S sequences, but also when we move off of these sequences towards more generic binaries. However, the formula should definitely be used with caution in an untested regime, especially when the trajectories are significantly altered by spin-orbit effects.

ACKNOWLEDGMENTS

We thank the referee for many helpful suggestions in improving the text. We gratefully acknowledge NSF for financial support from grants No. PHY-0722315, No. PHY-0722703, No. PHY-0714388, and No. PHY-653303. Computational resources were provided by Lonestar cluster at TACC and by NewHorizons at RIT.

APPENDIX A: POST-NEWTONIAN MODELING

Here we provide a brief post-Newtonian analysis of the configurations that maximize the recoil velocity for spin-

ning black holes. The spin-orbit-coupling (SO) contribution to the radiated linear momentum is given by Eq. (11).

We will restrict our analysis to planar orbits. Hence we have

$$\vec{v} = \dot{r}\hat{n} + r\omega\hat{\lambda}, \quad (\text{A1})$$

where $\hat{\lambda} = \hat{L}_N \times \hat{n}$, $\hat{L}_N = \vec{L}_N/|\vec{L}_N|$, ω is the orbital angular velocity, and $\vec{L}_N \equiv \mu(\vec{x} \times \vec{v})$ is the Newtonian orbital angular momentum. We shall take $\hat{L}_N \equiv \hat{z}$. Hence

$$\hat{\lambda} = \hat{z} \times \hat{n} \quad \text{and} \quad \hat{n} \times \hat{\lambda} = \hat{n} \times (\hat{z} \times \hat{n}) = \hat{z}. \quad (\text{A2})$$

We observe that the third and fourth terms in Eq. (11) only contribute to the recoil along the z -axis since

$$\hat{n} \times \vec{v} = r\omega\hat{z}. \quad (\text{A3})$$

This contribution to the recoil velocity might well be the leading one, hence, in order to maximize the total recoil we seek to align, as much as possible, the first two terms in Eq. (11) with the z -axis. This is achieved by having the spin of the black holes lie in the orbital plane, i.e.

$$\vec{\Delta} = \Delta_n\hat{n} + \Delta_\lambda\hat{\lambda}. \quad (\text{A4})$$

We then explicitly obtain the following products:

$$\vec{v} \times \vec{\Delta} = (\dot{r}\Delta_\lambda - r\omega\Delta_n)\hat{z}, \quad (\text{A5})$$

$$\hat{n} \times \vec{\Delta} = \Delta_\lambda\hat{z}, \quad (\text{A6})$$

$$\vec{v} \cdot \vec{\Delta} = \dot{r}\Delta_n + r\omega\Delta_\lambda. \quad (\text{A7})$$

Plugging this into Eq. (11) we find

$$\dot{\vec{P}}_{\text{SO}}^{\parallel} = -\frac{8}{15} \frac{\mu^2 m}{r^5} \{(2\dot{r}^2 - 4r^2\omega^2)\Delta_\lambda - 9\dot{r}r\omega\Delta_n\}\hat{z}. \quad (\text{A8})$$

This clearly displays the fact that the recoil will be maximized when Δ takes the maximum magnitude (equal mass and opposite maximally rotating black holes) and varies sinusoidally with its projection along the line joining

the holes. Note that if we define the angle between \hat{n} and $\vec{\Delta}$ as θ we can write the above equation as

$$\begin{aligned} \dot{\vec{P}}_{\text{SO}}^{\parallel} &= A(r)|\vec{\Delta}| \cos\theta + B(r)|\vec{\Delta}| \sin\theta \\ &= C(r)|\vec{\Delta}| \cos(\theta - \theta_0(r)). \end{aligned} \quad (\text{A9})$$

This $\cos\theta$ dependence in the recoil was the motivation for proposing the now-verified $\cos\Theta$ dependence in our empirical formula Eq. (2c) for the recoil.

Note that this analysis applies to the radiated linear momentum flux. Hence we have assumed that the larger the radiated linear momentum flux, the larger the net radiated linear momentum.

It is also interesting to see if the unexpectedly large magnitude of the maximum out-of-plane recoil, compared to the in-plane recoil, can be understood using the post-Newtonian expression for the radiated linear momentum, i.e. Eqs. (15) and (A8). To do this, we used the post-Newtonian formulae for the radiated linear momentum along with the numerical trajectories for runs with the spins in the plane and perpendicular to the plane. We found that the post-Newtonian formulae predicted that the maximum out-of-plane recoil will be approximately twice (almost 9/4) as large, rather than (the observed) ≈ 8 times as large, as the maximum in-plane recoil. Thus we see that the magnitude of the out-of-plane recoil arises from nonlinear dynamics at merger not fully captured by the post-Newtonian formalism. One may then conclude that, while the post-Newtonian approximation gives the correct dependence of the recoil on the physical parameters, such as the scaling of the recoil velocities with the components of the spins parallel and perpendicular to the angular momentum, it is much less accurate when describing the amplitude of the recoils. Thus we find that post-Newtonian formalisms provides the correct form for our semi-empirical formula (1), but does not provide accurate measurements of the magnitudes of the constants in that formula.

-
- [1] F. Pretorius, Phys. Rev. Lett. **95**, 121101 (2005).
[2] M. Campanelli, C. O. Lousto, P. Marronetti, and Y. Zlochower, Phys. Rev. Lett. **96**, 111101 (2006).
[3] J. G. Baker, J. Centrella, D.-I. Choi, M. Koppitz, and J. van Meter, Phys. Rev. Lett. **96**, 111102 (2006).
[4] M. Campanelli, C. O. Lousto, and Y. Zlochower, Phys. Rev. D **73**, 061501(R) (2006).
[5] J. G. Baker, J. Centrella, D.-I. Choi, M. Koppitz, and J. van Meter, Phys. Rev. D **73**, 104002 (2006).
[6] M. Campanelli, C. O. Lousto, and Y. Zlochower, Phys. Rev. D **74**, 041501(R) (2006).
[7] M. Campanelli, C. O. Lousto, and Y. Zlochower, Phys. Rev. D **74**, 084023 (2006).
[8] M. Campanelli, C. O. Lousto, Y. Zlochower, B. Krishnan, and D. Merritt, Phys. Rev. D **75**, 064030 (2007).
[9] F. Pretorius, Classical Quantum Gravity **23**, S529 (2006).
[10] F. Pretorius and D. Khurana, Classical Quantum Gravity **24**, S83 (2007).
[11] J. G. Baker, J. R. van Meter, S. T. McWilliams, J. Centrella, and B. J. Kelly, Phys. Rev. Lett. **99**, 181101 (2007).
[12] B. Bruegmann *et al.*, arXiv:gr-qc/0610128 [Phys. Rev. D (to be published)].

- [13] A. Buonanno, G. B. Cook, and F. Pretorius, *Phys. Rev. D* **75**, 124018 (2007).
- [14] J. G. Baker *et al.*, *Phys. Rev. D* **75**, 124024 (2007).
- [15] M. A. Scheel *et al.*, *Phys. Rev. D* **74**, 104006 (2006).
- [16] J. G. Baker, M. Campanelli, F. Pretorius, and Y. Zlochower, *Classical Quantum Gravity* **24**, S25 (2007).
- [17] P. Marronetti *et al.*, *Classical Quantum Gravity* **24**, S43 (2007).
- [18] H. P. Pfeiffer *et al.*, *Classical Quantum Gravity* **24**, S59 (2007).
- [19] M. Campanelli, *Classical Quantum Gravity* **22**, S387 (2005).
- [20] F. Herrmann, D. Shoemaker, and P. Laguna, arXiv:gr-qc/0601026.
- [21] J. G. Baker *et al.*, *Astrophys. J.* **653**, L93 (2006).
- [22] C. F. Sopuerta, N. Yunes, and P. Laguna, *Phys. Rev. D* **74**, 124010 (2006).
- [23] J. A. Gonzalez, U. Sperhake, B. Bruegmann, M. Hannam, and S. Husa, *Phys. Rev. Lett.* **98**, 091101 (2007).
- [24] C. F. Sopuerta, N. Yunes, and P. Laguna, *Astrophys. J.* **656**, L9 (2007).
- [25] F. Herrmann, I. Hinder, D. Shoemaker, and P. Laguna, *AIP Conf. Proc.* **873**, 89 (2006).
- [26] F. Herrmann, I. Hinder, D. Shoemaker, and P. Laguna, *Classical Quantum Gravity* **24**, S33 (2007).
- [27] F. Herrmann, I. Hinder, D. Shoemaker, P. Laguna, and R. A. Matzner, arXiv:gr-qc/0701143.
- [28] M. Campanelli, C. O. Lousto, Y. Zlochower, and D. Merritt, *Astrophys. J.* **659**, L5 (2007).
- [29] M. Koppitz *et al.*, *Phys. Rev. Lett.* **99**, 041102 (2007).
- [30] D.-I. Choi *et al.*, *Phys. Rev. D* **76**, 104026 (2007).
- [31] J. A. Gonzalez, M. D. Hannam, U. Sperhake, B. Brügmann, and S. Husa, *Phys. Rev. Lett.* **98**, 231101 (2007).
- [32] J. G. Baker *et al.*, *Astrophys. J.* **668**, 1140 (2007).
- [33] M. Campanelli, C. O. Lousto, Y. Zlochower, and D. Merritt, *Phys. Rev. Lett.* **98**, 231102 (2007).
- [34] E. Berti *et al.*, *Phys. Rev. D* **76**, 064034 (2007).
- [35] W. Tichy and P. Marronetti, *Phys. Rev. D* **76**, 061502 (2007).
- [36] F. Herrmann, I. Hinder, D. M. Shoemaker, P. Laguna, and R. A. Matzner, *Phys. Rev. D* **76**, 084032 (2007).
- [37] B. Brügmann, J. A. González, M. Hannam, S. Husa, and U. Sperhake, arXiv:0707.0135.
- [38] J. D. Schnittman *et al.*, arXiv:0707.0301.
- [39] B. Krishnan, C. O. Lousto, and Y. Zlochower, *Phys. Rev. D* **76**, 081501 (2007).
- [40] K. Holley-Bockelmann, K. Gültekin, D. Shoemaker, and N. Yunes, arXiv:0707.1334.
- [41] D. Pollney *et al.*, *Phys. Rev. D* **76**, 124002 (2007).
- [42] I. H. Redmount and M. J. Rees, *Comments Astrophys.* **14**, 165 (1989).
- [43] D. Merritt, M. Milosavljevic, M. Favata, S. A. Hughes, and D. E. Holz, *Astrophys. J.* **607**, L9 (2004).
- [44] A. Gualandris and D. Merritt, arXiv:0708.0771.
- [45] R. C. Kapoor, *Pramana* **7**, 334 (1976).
- [46] M. J. Fitchett, *Mon. Not. R. Astron. Soc.* **203**, 1049 (1983).
- [47] L. E. Kidder, *Phys. Rev. D* **52**, 821 (1995).
- [48] M. Campanelli, C. O. Lousto, Y. Zlochower, and D. Merritt, *Phys. Rev. Lett.* **98**, 231102 (2007).
- [49] S. Brandt and B. Brügmann, *Phys. Rev. Lett.* **78**, 3606 (1997).
- [50] M. Ansorg, B. Brügmann, and W. Tichy, *Phys. Rev. D* **70**, 064011 (2004).
- [51] Y. Zlochower, J. G. Baker, M. Campanelli, and C. O. Lousto, *Phys. Rev. D* **72**, 024021 (2005).
- [52] T. Nakamura, K. Oohara, and Y. Kojima, *Prog. Theor. Phys. Suppl.* **90**, 1 (1987).
- [53] M. Shibata and T. Nakamura, *Phys. Rev. D* **52**, 5428 (1995).
- [54] T. W. Baumgarte and S. L. Shapiro, *Phys. Rev. D* **59**, 024007 (1998).
- [55] E. Schnetter, S. H. Hawley, and I. Hawke, *Classical Quantum Gravity* **21**, 1465 (2004).
- [56] carpet_web, fixed Mesh Refinement with Carpet: <http://www.tat.physik.uni-tuebingen.de/~schnette/carpet/>.
- [57] M. Alcubierre, B. Brügmann, P. Diener, M. Koppitz, D. Pollney, E. Seidel, and R. Takahashi, *Phys. Rev. D* **67**, 084023 (2003).
- [58] C. Gundlach and J. M. Martin-Garcia, *Phys. Rev. D* **74**, 024016 (2006).
- [59] J. Thornburg, *Classical Quantum Gravity* **21**, 743 (2004).
- [60] O. Dreyer, B. Krishnan, D. Shoemaker, and E. Schnetter, *Phys. Rev. D* **67**, 024018 (2003).
- [61] M. Campanelli and C. O. Lousto, *Phys. Rev. D* **59**, 124022 (1999).
- [62] C. O. Lousto and Y. Zlochower, *Phys. Rev. D* **76**, 041502(R) (2007).
- [63] A. G. Wiseman, *Phys. Rev. D* **46**, 1517 (1992).
- [64] J. Baker, M. Campanelli, C. O. Lousto, and R. Takahashi, *Phys. Rev. D* **65**, 124012 (2002).
- [65] J. Baker, B. Brügmann, M. Campanelli, and C. O. Lousto, *Classical Quantum Gravity* **17**, L149 (2000).
- [66] J. Baker, B. Brügmann, M. Campanelli, C. O. Lousto, and R. Takahashi, *Phys. Rev. Lett.* **87**, 121103 (2001).
- [67] J. Baker, M. Campanelli, and C. O. Lousto, *Phys. Rev. D* **65**, 044001 (2002).
- [68] J. G. Baker, M. Campanelli, C. O. Lousto, and R. Takahashi, *Phys. Rev. D* **69**, 027505 (2004).
- [69] M. Campanelli, B. Kelly, and C. O. Lousto, *Phys. Rev. D* **73**, 064005 (2006).